Flux Investigations for Neutrino Experiments in the NuMI Beam

A thesis submitted in partial fulfillment of the requirements for the degree of Bachelor of Science degree in Physics from the College of William and Mary

by

Paulo Jared Black

Advisor: Patricia Vahle

Senior Research Coordinator: Gina Hoatson

Date: May 11, 2015

Flux Investigations for Neutrino Experiments in the NuMI Beam

Paulo J. Black

Advisor: Patricia Vahle

Senior Research Coordinator: Gina Hoatson

May 11, 2015

Abstract

The Near Detector of the MINOS neutrino experiment is currently producing data which differs from the extant predictive simulation. We have reconstructed the simulations, then created a new simulation by weighting the result of the simulation with the difference between the predicted results and the actual results. We then analyze the momentum components of the new simulation to determine how much each component of the simulation needs to be modified to match experimental data. We conclude that the simulation for the longitudinal component of pion momentum is responsible for our error, we examine the modeling of individual areas of the cross-section of the Near Detector. Examining the corresponding regions of the Near Detector's experimental results, we hope to find new constraints on the beam flux to use in a global fit of the Monte Carlo simulation used in describing the Near Detector's spectra.

1 Introduction

Over the last several decades neutrino beams have become more prevalent not just in understanding of the neutrino as a particle in and of itself, but also for probing and understanding of more fundamental physical relationships in the standard model. The techniques used to create these beams have adapted and improved over time, and there exist today a variety of methods by which to create an experimentally functional neutrino beam. Developed simultaneously by CERN, KEK, FermiLab, and other laboratories, the neutrino beam has seen several upgrades throughout the last 50 years. The contemporary beam is one that involves the construction of an intense neutrino beam that passes several hundred kilometers through the earth to a distant far detector in order to increase purity of data and reduce interference. [1]

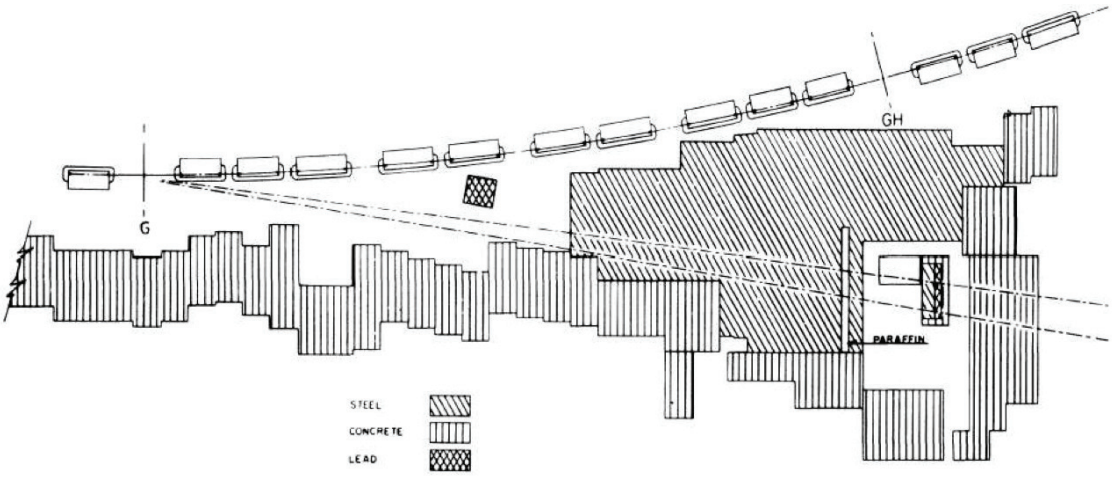

Figure 1: A cursory blueprint of the first neutrino beam ever created at the Brookhaven National Laboratory in 1962. The diagonal lines represent steel sections, horizontal lines represent concrete, and the dots represent lead sections.

1.1 Neutrino Beam Production

The modern standard "conventional neutrino beam" is one in which a high energy proton beam collides with a nuclear target, producing a pion beam which is then focused into a (more) coherent beam, eventually decaying into neutrinos. The first such beam was created in 1962 at Brookhaven National Laboratory by a team of high energy physicists seeking to better understand the neutrino, the blueprint of which is found in Figure 1. This first beam utilized a straight section of a pre-existing particle accelerator to direct a 15GeV proton beam to strike a Beryllium target, emitting pions from the target which would then pass through a 21m drift space before striking a 13.5m iron shield, behind which was a 10-ton aluminum spark chamber to detect incident neutrinos. [2] While impressive, by modern standards this beam has many difficulties. The pions produced by striking this target were not directed towards the detector due to non-linearity in particle decay, resulting in severe losses. The difference in neutrino flux between a perfectly focused and a completely unfocused pion beam is on the order of 25. [1]. Over the last several decades, many introductions including focusing lenses, two detector experiments, and fast-extracting, external proton beams have resulted in much higher quality experiments.

Focusing lenses, sometimes called magnetic focusing horns, are perhaps the most relevant addition to the neutrino beam for the present work. The first of such lenses was called a Van Der Meer Lens (Figure 2). As can be seen, it has a conical geometry, contrasted to the horns used in the NuMI Beam in the MINOS Experiment, which features two parabolic horns seen in Figure 3. The details concerning both geometries, their differences and effects as well as those of other available geometries is discussed at length in Kopp [1].

While these types of beams are in use across the world, we are interested primarily in discussing the beam used in the MINOS experiment at Fermilab. The produced pions (and secondary kaons) from the target interaction are boosted forward with a divergence described by $d^2\phi/dp_t dx_f$ where p_t is the transverse momentum of the particle

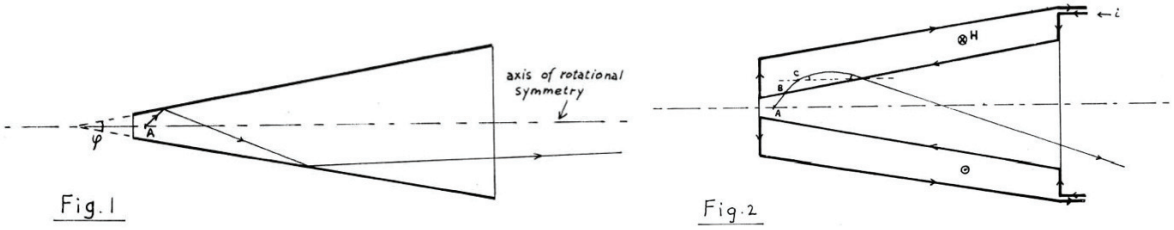

Figure 2: A schematic of the first magnetic focusing lens, the Van Der Meers Lens. These focusing horns helped capture significantly more pions as they were emitted from the nuclear target, refocusing back into the beam incident on the detector.

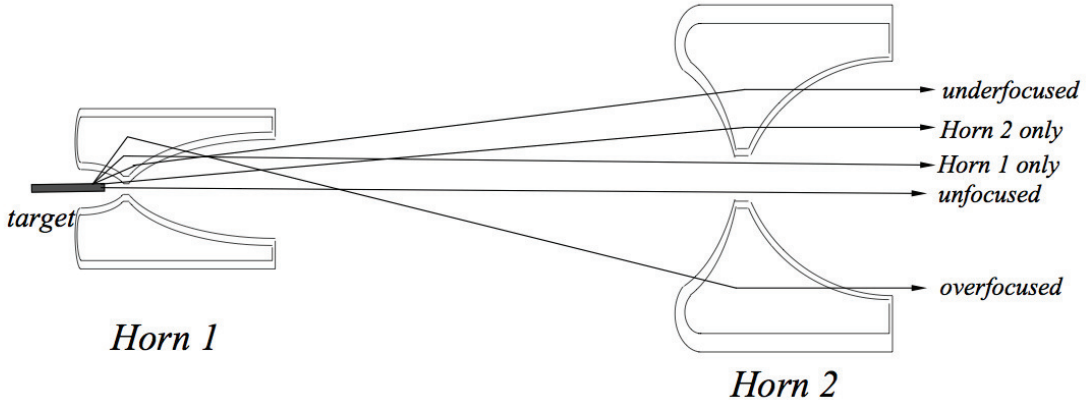

Figure 3: A schematic of the parabolic focusing horns utilized in the NuMI Beam, the neutrino source for the MINOS experiment.

relative to the beam's axis and $x_f \approx p_l/p_{proton}$ is the particle's longitudinal momentum (after interaction with the target) divided by the momentum of the incident proton beam. A schematic diagram for the component momenta can be seen in Figure 4. These pions and kaons are focused towards the center longitudinal axis with the focusing lens and decay into neutrinos along some drift space before the near detector of the set-up. The non-neutrino particles are removed from the beam with a muon filter (essentially a rock target which only transmits a percentage of the incident particles) integrated in the system. The energy of a neutrino created by this system can be approximated with Equation 1 and the flux by Equation 2. The term of angle of decay in each is θ, and is the relevant term to our considerations. [3]

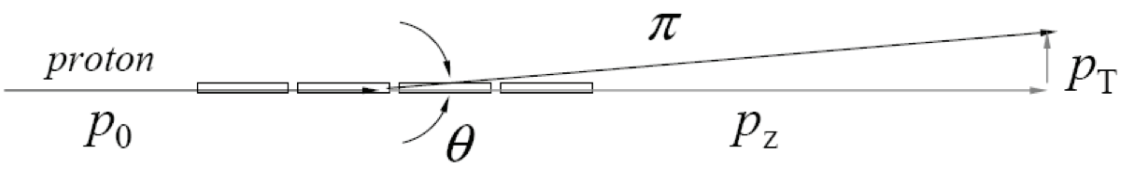

Figure 4: A schematic representation of the transverse and longitudinal components of the momenta of the pions which will eventually decay into the detected neutrinos.

$$E_\nu \approx \frac{0.43 E_\pi}{1 + \gamma^2 \theta_\nu^2} \tag{1}$$

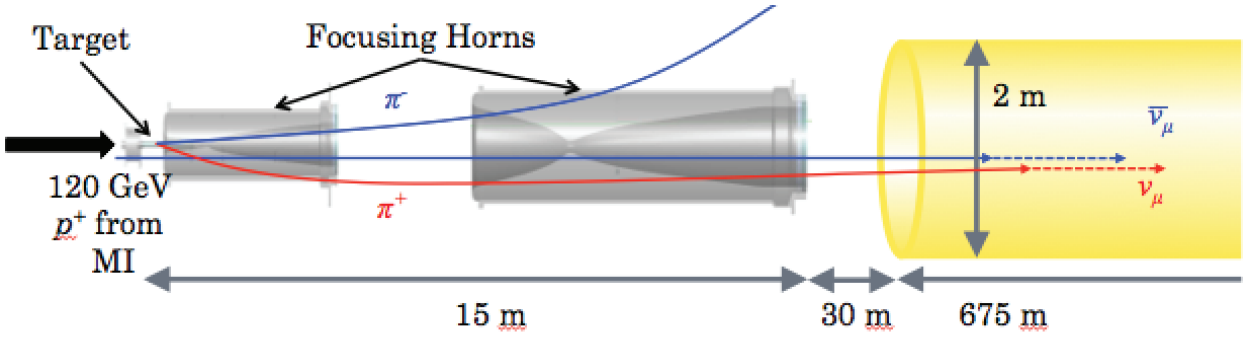

Figure 5: A schematic representation of the long range, proton to pion to neutrino beam setup used in MINOS.

$$\phi_\nu = \frac{A}{4\pi z^2} \left(\frac{2\gamma}{1 + \gamma^2 \theta^2} \right)^2 \tag{2}$$

1.2 The MINOS Experiment

A schematic outline of the neutrino beam is shown in Figure 5, the one used in the Fermilab MINOS experiment. The incident proton beam strikes the target with initial energy of 120 GeV, producing pions of varying composite momenta. These pions are then refocused into a beam, then they decay into muon neutrinos, passing through the muon filter before undergoing the long journey to the far detector. As discussed briefly, the use of geometrically varying lenses (referred to as focusing horns) has drastically improved the quality of neutrino experiments. Exiting pions have a large longitudinal momentum from their original trajectory as protons, in addition to the change in momentum from the emission of the pion from the target. This produces the transverse momentum according to $p_t \approx 2p_\pi/\gamma$, which is then ideally negated by a proportional "kick" in the opposite direction by a magnetic field proportional to the distance from the beam's axis, directing the wayward pion back toward the central axis. The MINOS experiment utilizes the parabolic horns that can be seen in Figure 5.

2 Experimental Data

The energy of a neutrino created by this system can be approximated with Equation 1. What is measured in the two detectors used by MINOS is the energy of each detected neutrino, as well as the count of interacting neutrinos with which the number of neutrinos expected per unit area, or the neutrino flux, is determined (see Equation 2). Both the neutrino energy and flux are dependent on the angle of decay of the pion into a neutrino (θ). This angle itself is dependent on the effect the focusing lens has had on the momentum of the pion prior to decay. The effect of the lens is determined

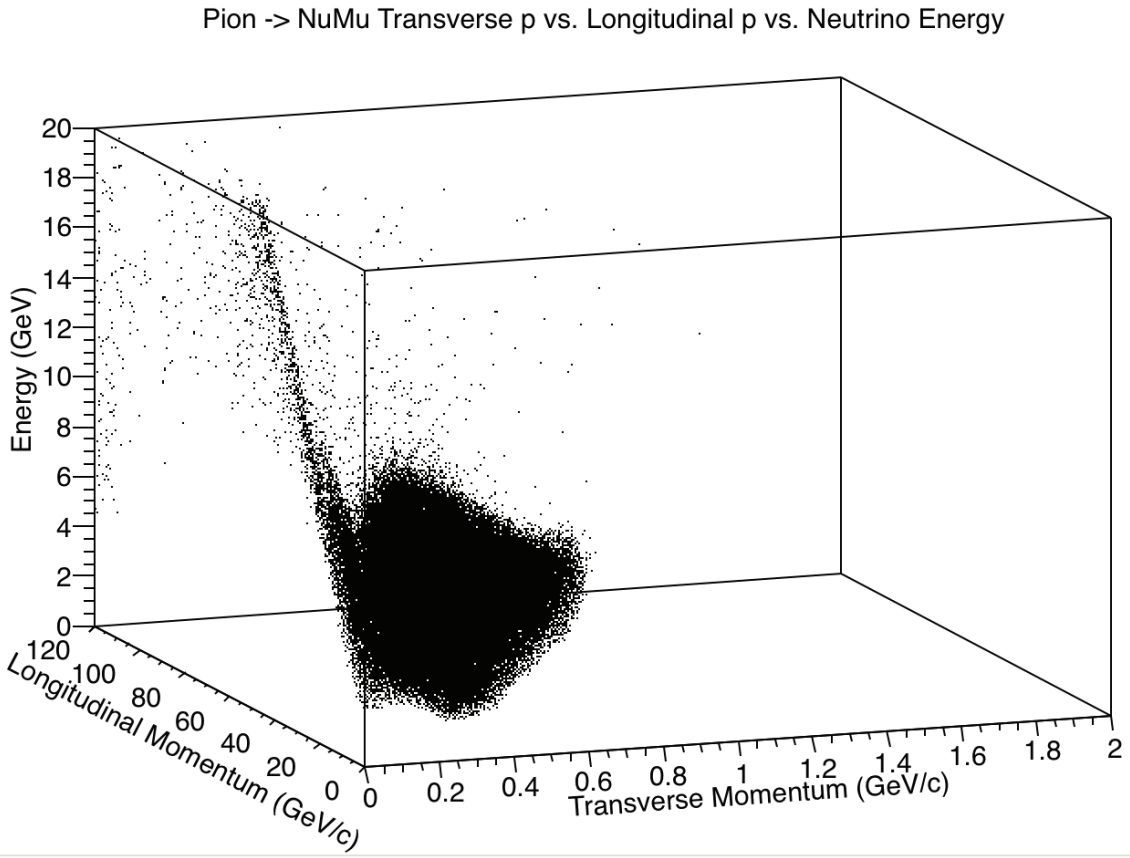

Figure 6: A histogram displaying the Pion E v p_t v p_l, (Energy, transverse momentum and longitudinal momentum respectively.

by the momentum of the pion upon exiting the nuclear target, particularly the transverse momentum, which influences how far from the center longitudinal axis the pion deviates and therefore for how long it is exposed to the magnetic field of the lens. We use a simulation which is essentially constructed in reverse order to attempt to predict the energy spectrum of detected neutrinos in the near detector. By knowing the incident proton beam energy (120GeV) we simulate the divergence and momentum of pions exiting the nuclear target as well as their subsequent refocusing towards the center axis. From here, the energy of the neutrino is calculated with a Monte Carlo simulation using Equation 1 and a distribution of detected neutrino properties can be calculated.

The simulated three dimensional plot of Pion Energy versus Longitudinal momentum (x_f) versus Transverse momentum (p_t), shown in Figure 6, is the result of the current best predictive code for the actual data recorded during MINOS experiments. Using this plot we are able to make comparisons between the data recorded from experiment and our predicted distribution of neutrino energy. In Figure 7 we see a 2-D projection of Figure 6 onto the momenta axes. This gives us a better look at how many neutrino events (the color spectrum) are predicted to carry what momentum values.

Figure 8 contains a comparison of the number of events versus energy readings of the real data (black) and the simulated data (red). Noting that the energy for our simulation was generally higher than experiment, we sought to discover which

component of our simulation was responsible for the difference. The sharp spike seen at the value corresponding to 5 GeV on the X axis is an artifact from the histogram binning process and is unrelated to the actual simulation at hand.

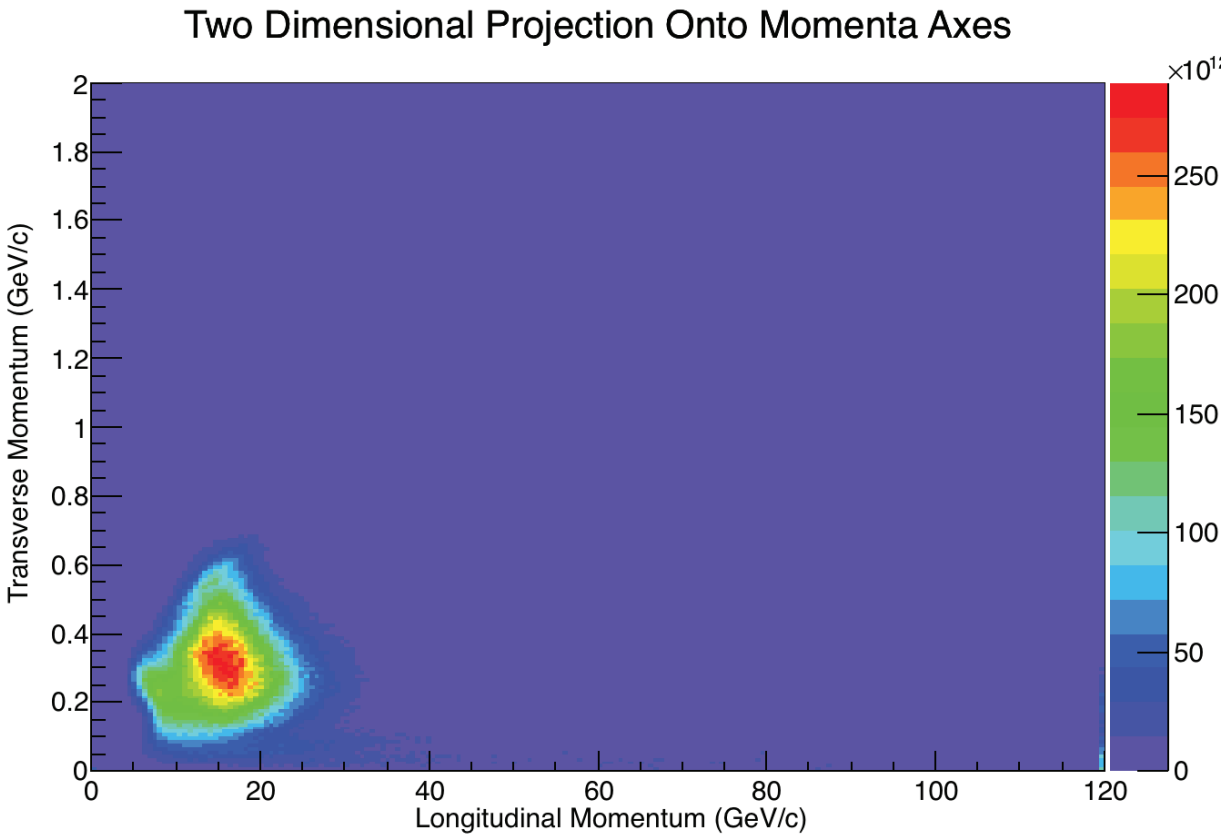

Figure 7: The 2D projection of Fig 2. onto the momenta axes. The color distribution corresponds to number of events in that bin.

3 Flux Investigations for Neutrino Experiments in the NuMI Beam

It is appropriate to divide our work into two phases. The first phase is concerned with an overall comparison of the simulation and the experiment in order to determine the source of our error on a superficial level. As we have seen from the above section, the first step in breaking down the predictions for the energy spectrum is understanding the predictions for the momenta of the pions which decay into our detected neutrinos. We attempted to discern between the predictions for the two component momenta in the hopes of isolating the erroneous portion of our simulation.The second phase is concerned with further probing of our simulation through more precise comparisons between it and the experimental data. This is made possible by the conclusion of the first phase. We examined the energy spectra across various small sections of the cross section of the Near Detector, both in our simulation and in the experiment, under an

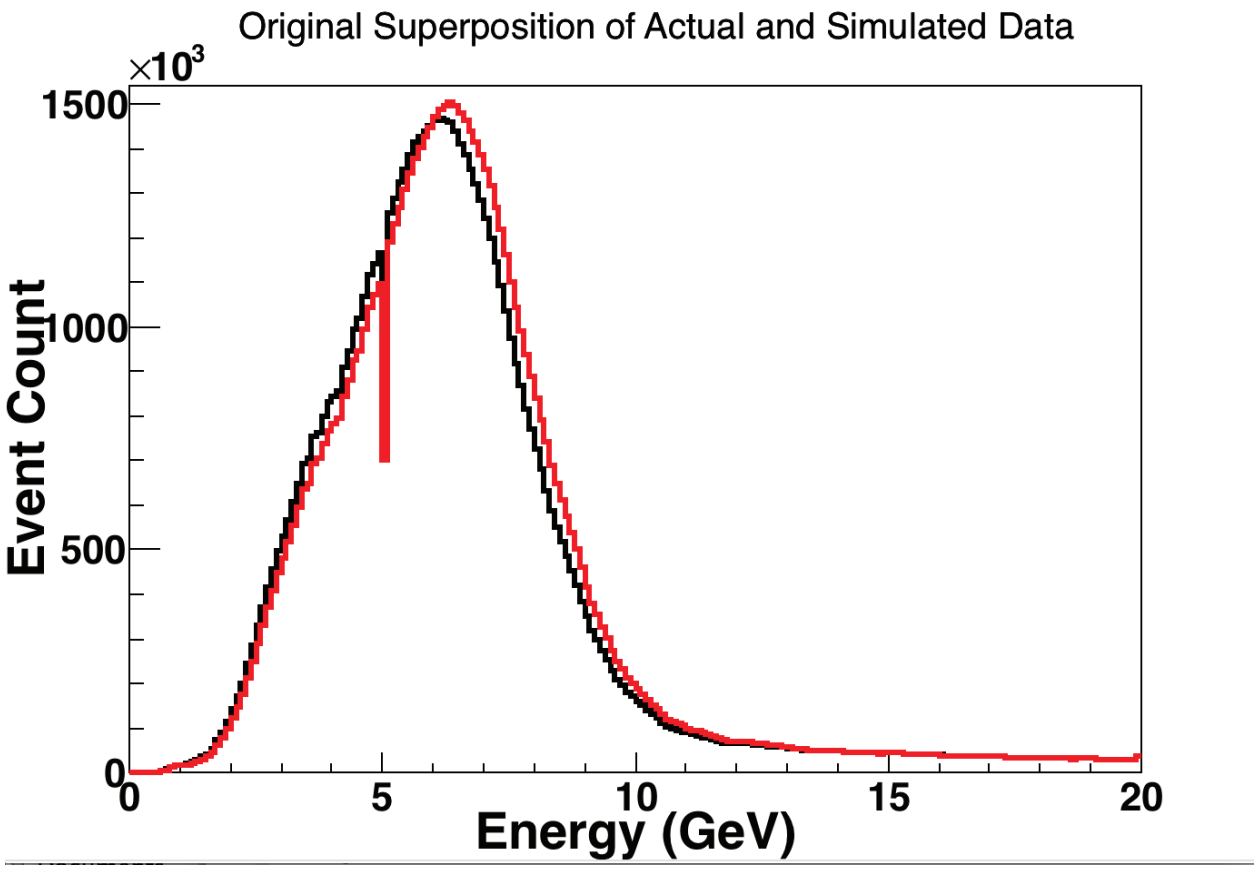

Figure 8: A superimposition of our actual data for Neutrino event count versus energy (black) and the Monte Carlo simulated data for the same conditions (red).

ansatz that the discrepancy was due to an error which would manifest itself in the physical position of our simulated beam.

We utilized C+ and ROOT, a library developed at CERN for use in High Energy Physics experiments, to conduct the simulations. The majority of the involved labor was concerned with creating complicated code to manipulate and investigate the simulated and experimental data.The graphs present in this paper are a product of that labor.

4 First Phase: Analysis of Momenta

Our proposed method for discovering the responsible component of momentum was to find a ratio between our recorded and simulated data, then weight our simulated data to fit the real data. With this weighted simulation we could compare projections onto each momentum axis of weighted and unweighted simulation data to determine which saw the greatest change upon weighting, and therefore which component was more responsible for the discrepancy in our simulation. When we here speak of longitudinal momentum and transverse momentum it is important to note that we are discussing x_f and p_t respectively (as they are referred to in Figures 6 and 7) as well as Equations 1 and 2.

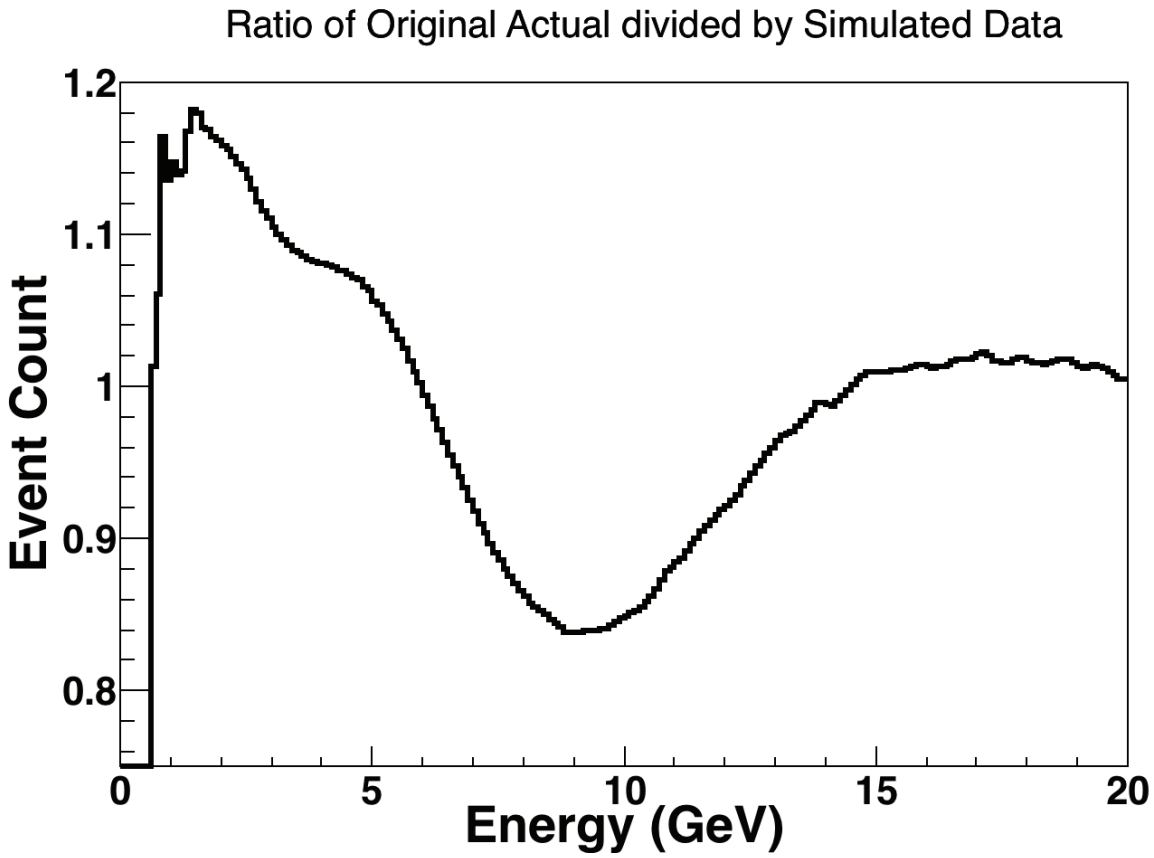

Figure 9: The ratio of the two Z projections of actual data divided by simulated data.

The first step was to divide the actual data by our simulated data in order to find a weight with which to change our simulated data in order to fit the actual data. The result of this division is in Figure 9. We were then able to correspond each bin along the energy axis of the ratio histogram (Fig. 9) with each bin of the energy axis in our original 3D simulation (Fig. 6). By taking the 2D projection of each Z bin in Figure 6 and weighting it with the corresponding ratio bin, we were able to artificially create a similar histogram that described our experimental results. A two dimensional projection, similar to that in Figure 7, was created for this new weighted simulation, followed by a two dimensional ratio of the two histograms, shown in Figure 10.

Finally, in order to examine the culprit component, we created projections onto both the transverse momentum axis and the longitudinal momentum axis of both weighted and unweighted simulations. The transverse momenta were then superimposed as were the longitudinal momenta as displayed in Figure 11. Below the two superpositions are ratios of each, the first ratio histogram being the weighted longitudinal momentum divided by unweighted longitudinal momentum, the second being weighted transverse momentum divided by unweighted transverse momentum.

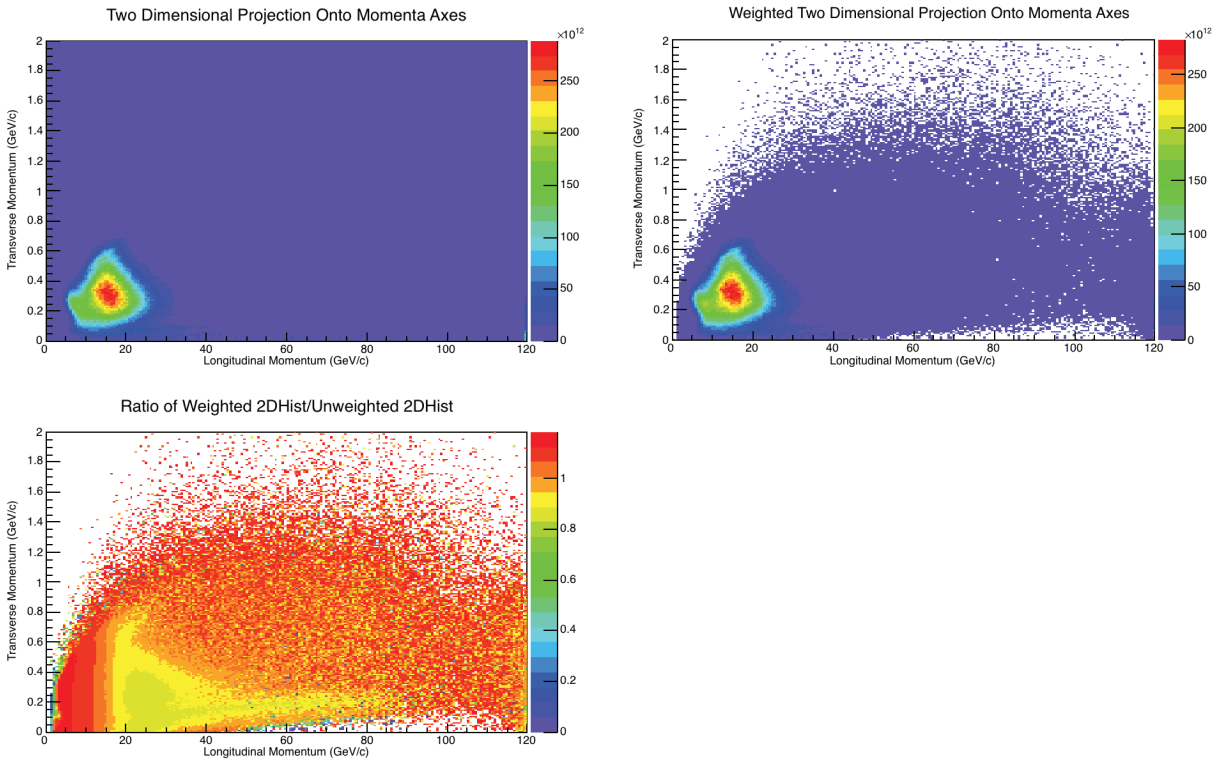

Figure 10: Top Left: Unweighted 2D Projection of Simulated Data (same as Figure 3.) Top Right: Weighted 2D Projection of Simulated Data. Bottom Left: Ratio of Weighted Divided by Unweighted Simulated Data. Color units are event count in first two histograms, and dimensionless ratio in bottom left histogram.

4.1 Discussion of the First Phase

We see several indications that the component responsible for the difference in energy values of simulated and experimental data is in fact, longitudinal momentum or x_f. The first is that in the bottom left histogram in Figure 10 we see a band like pattern in the transverse axis. The discontinuities come as we move along the x axis, showing the longitudinal momentum corresponds to variation in number of events between the unweighted and weighted simulations. Upon closer investigation, we see that in Figure 11 the ratio between longitudinal momenta displays a ratio with a strikingly similar curve to that found in Figure 9, deviating quite far from a desired ratio of 1, whereas the transverse ratio follows quite close to this desired value.

From these simulations we can conclude that in our simulated experiment, the x_f (longitudinal) component is simulated improperly, resulting in data that deviates from experimental data by showing overall higher energies. At this point we have succeeded in the first phase's goal of finding the characteristics of our error which serve to isolate it one further order from the superficial error in our simulation. As there are a variety of simulations responsible for predictions of the longitudinal momenta spectrum, further troubleshooting is required. We suspect that the most likely culprit is the model we use to represent the magnetic focusing horns' redirection of the pions straying from the beam's original axis.

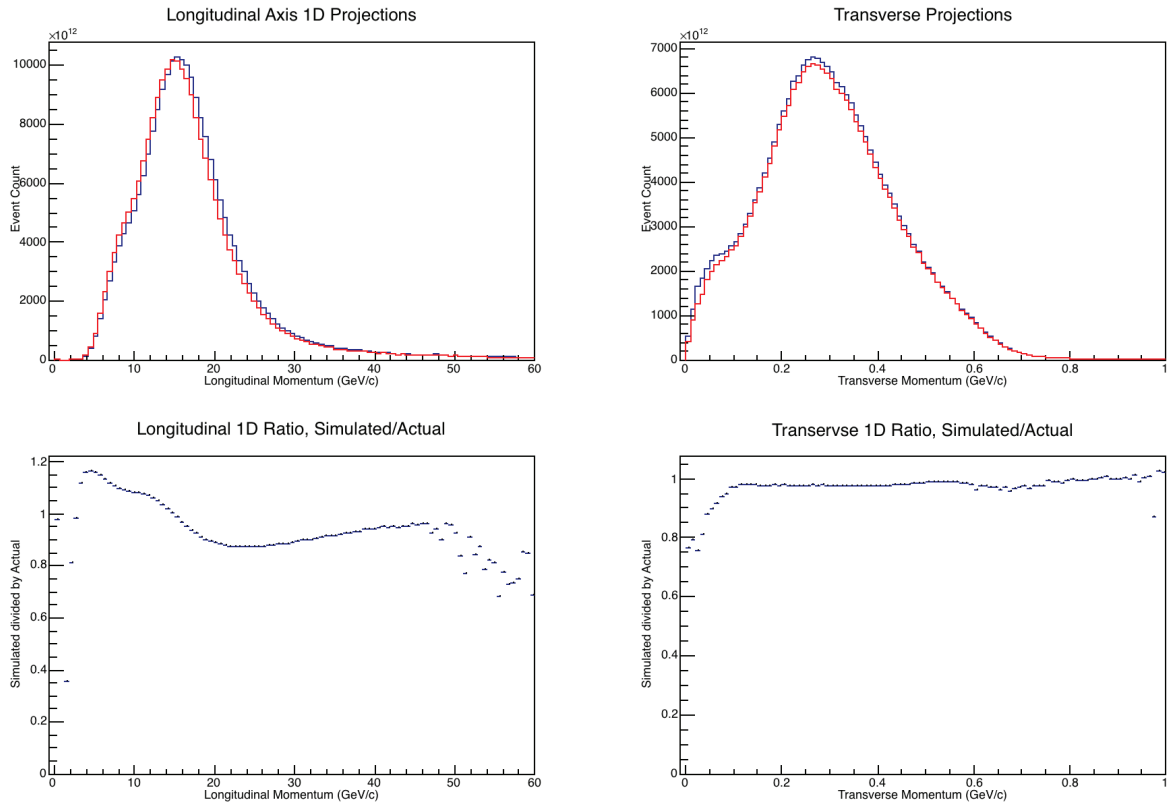

Figure 11: Top Left: Unweighted projection (red) and weighted projection (blue) of longitudinal momentum x_f. Top Right: Unweighted projection (red) and weighted projection (blue) of transverse momentum p_t. Bottom Left: Ratio of weighted divided by unweighted simulated data for longitudinal momentum x_f. Bottom Right: Ratio of weighted divided by unweighted simulated data for transverse momentum p_t.

5 Second Phase: Troubleshooting

Having determined conclusively that the predicted values for longitudinal momenta were responsible for the overall defects in the simulation we were able to begin looking for feautures in the data that may help us develop a better flux model. The first step of this process was to examine the simulation once again, this time looking at the predicted energy spectrum across different positions in the detector. By analyzing the predicted data across certain areas of the Near Detector and comparing them to the corresponding areas from the experimental data, we hope to isolate the cause of our discrepancy. If the significant variation between the two occurs farther from the beam center, we might have further evidence that the modeling of the refocusing effect from the magnetic horns is indeed our source of error.

5.1 Predicted Energy Across 2D Sections of the Near Detector

Previously, as can be seen in the red plot in Figure 8, we modeled the overall predicted energy spectrum for neutrinos incident on the Near Detector (and in this figure, superimposed it with the black plot, which is the physically measured energy spectrum).

Returning to our simulation, we designated specific areas across the cross section of the detector to analyze what was being simulated at different areas of the detector. The way our simulation is designed, we are able to specify a position in x-y-z coordinates and then examine an area about this point. This simulation accounts only for beam effect corrections, ignoring geometric and detector contributions. In using this particular simulation rather than the complete one, we sought to perform a rudimentary check to determine if we could in fact see the effect of the changing angle of the beam in the simulation before moving to the more complicated, complete comparison.

The Z axis represents longitudinal position, as in the position of the detector in relation to the source of incident particles. This position remained constant. The X-Y plane represents the cross-sectional area of the detector, as such this was our plane of interest. In order to have a good idea of the simulated spectra at each position, we wanted to have a set of areas which could be compared relative to one another, thus we held the Y position, representing the vertical axis of the detector constant. We then moved our area laterally, across the X axis, in steps of 25cm at a time, from x = 0 to x = 300, followed by the "extreme" cases x = 500cm, x = 1000cm and x = 5000cm. The area covered by each step along the X direction is a square, .5m x .5m in size. The resulting 16 histograms can be found in Figure 12.

From these plots it can be seen that as we move off the beam's center axis, both the mean and the number of entries decreases, as expected. Knowing that the effect could indeed be seen in the simulation, we continued the investigation using the complete simulation in comparison with measured spectra from the detector.

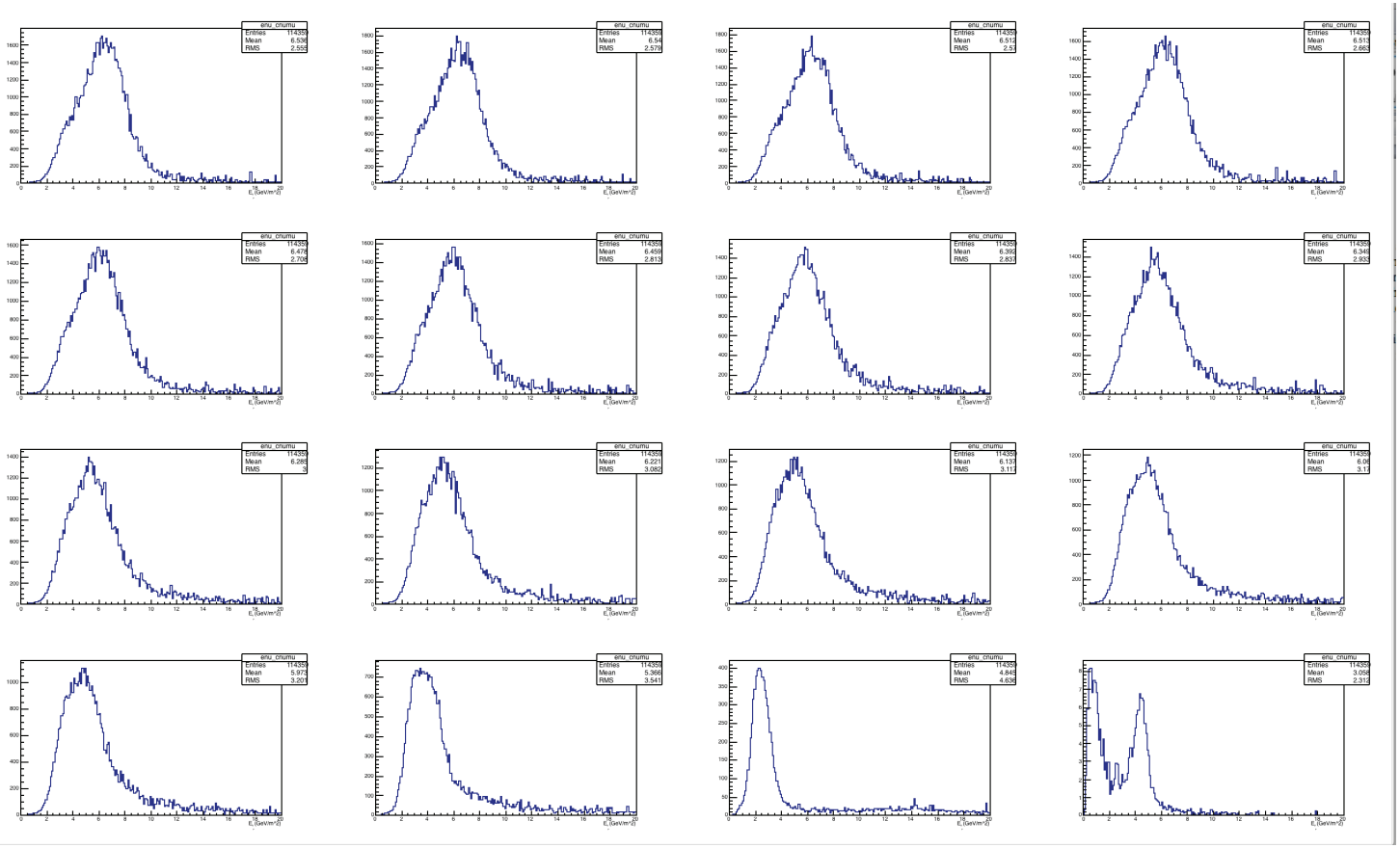

Figure 12: Starting at the top left corner and moving left to right, we see the varying predicted energy spectra dependent on position of the Near Detector. The longitudinal distance from the beam source was held constant, as was the vertical position along the cross section of the detector. The area of interest was shifted in steps of 25cm along the horizontal axis of the detector from x = 0cm (center position) to x = 300cm. The final three histograms represent the areas at x = 500cm, x = 1000cm and x = 5000cm respectively. It can be seen clearly here that the mean energy and number of entries decreases when moving off beam axis, as expected. Along each Y axis is the event count, and along each X axis is energy in GeV (on the order of roughly 5GeV. Of importance is the decrease of event count and energy relative to the top right histogram, rather than the individual values of each plot.

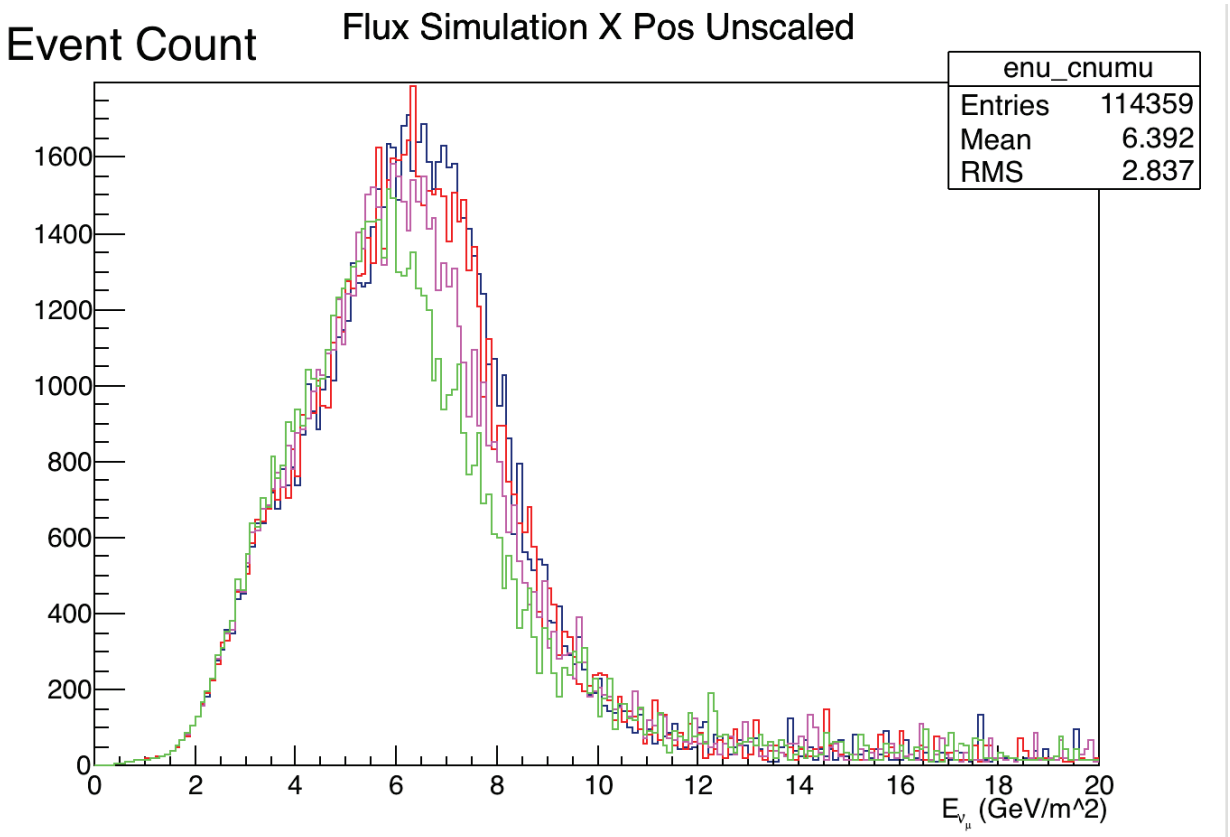

Figure 13: Beam Angle Simulation Unscaled, colors representing position (in decreasing order) at origin, .5m from origin, 1m from origin, 1.5m from origin

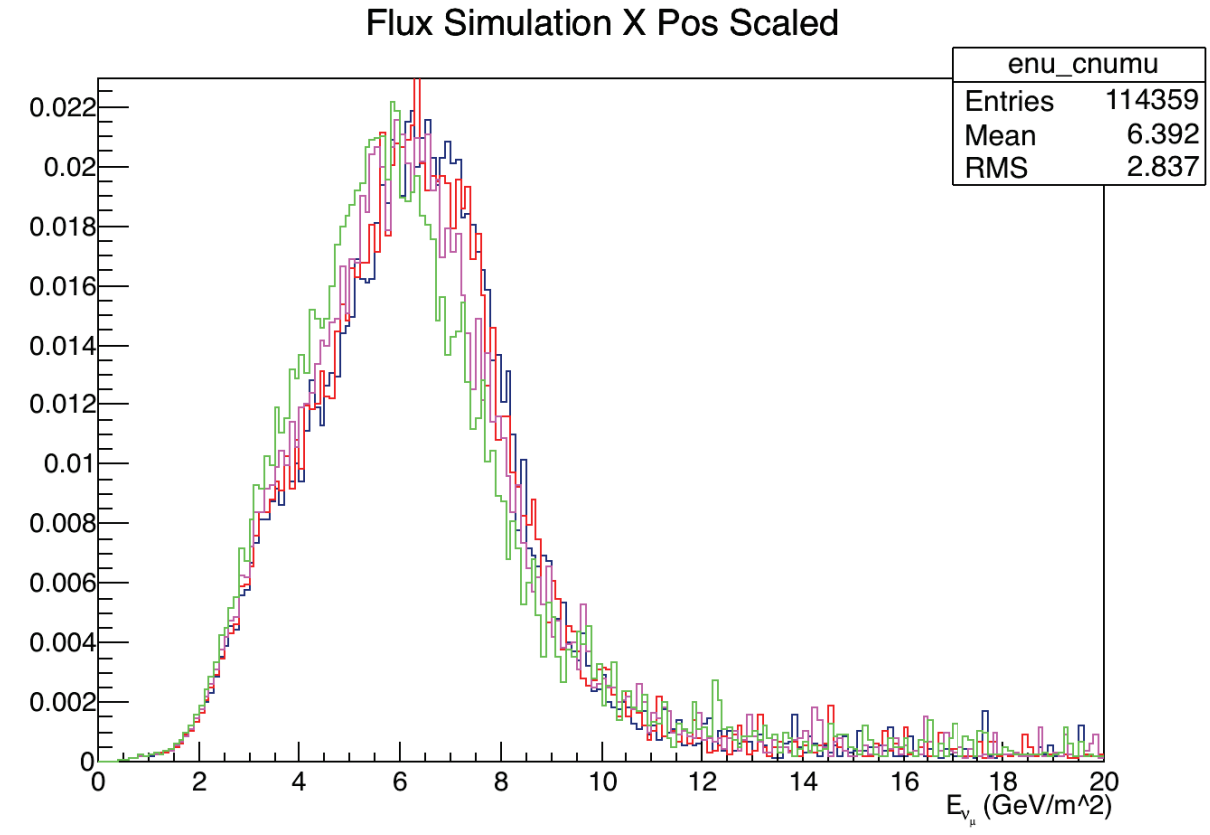

Figure 14: Beam Angle Simulation Scaled, colors representing position (in decreasing order) at origin, .5m from origin, 1m from origin, 1.5m from origin

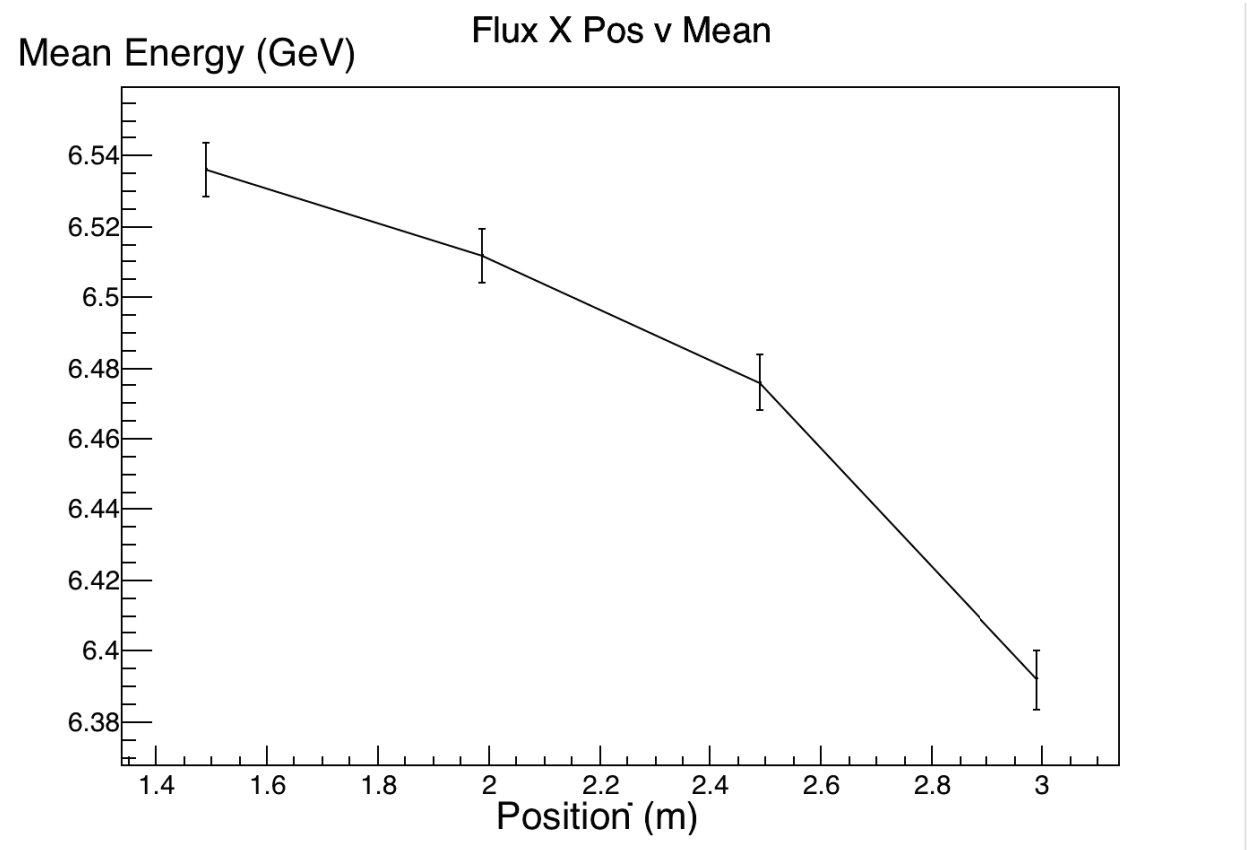

Figure 15: Flux Mean v Position

5.2 Analysis of Experimental Positional Data

We inspected MINOS experimental data, stored at Fermilab, examining the different energy spectra measured across different areas of the detector. Beginning at the position for beam-center, we shifted our area of interest (this time a circle of radius .5m) in both directions across the X and Y axes in steps of .5m at a time. Due to interesting results in our analysis, we decided to redo our examination from the previous section. Using a simulation with a more sophisticated and detailed procedure for calculating the positionally dependent energy spectra, we were able to compare the experimental data with a model that took into full consideration all aspects of the mechanism involved, including not just beam effects but also detector geometry and effects. These inclusions become necessary at this point due to our direct comparisons of the simulation to the detector measurements.

The comparisons necessitated an extensive amount of modeling, the results of which can be found below. We have provided on each page a comparison between the portion of cross-sectional areas examined in the experimental data as well as the simulated data. For the X axis histograms, starting from the red curve, the blue, then purple, then green curves are each plots centered .5m farther from the axis in their respective directions from the last plot, the final step being an increment of .4m due to experimental constraints discussed below. For Y axis histograms we have done the same thing, with all steps being in the full .5m increment. We have also included, for both X and Y, experimental and simulated analyses, a 1D plot of both the Number of Events vs Position of the Beam (Entries vs Pos) and a plot of Energy Mean vs Position of the Beam (Mean vs Pos) in Figures 32 through 39.

6 Discussion of the Second Phase

As the cosmetic structure of each plot is identical, the structures will be described here rather than individually in each figure. In the sixteen spectrum plots, all X axes describe the magnitude of energy, whereas the Y axis corresponds to the number of detected neutrinos. There is in each plot, in order of descending magnitude, a blue, red, purple, and green histogram. These correspond, respectively, to the origin, followed by a step of $.5m$ in the specified direction, followed by another step, followed by the final step of $.4m$ for X and a normal step of $.5m$ for Y. The structures for the two flux simulation plots are identical to these previous plots as well, and move in steps of $.5m$ with the same color progression.

It is clear from the unscaled plots that the number of entries (the overall size of the histogram) decreases as we move farther from the origin. From the scaled histograms we see that in normalizing our unscaled plots there is also an overall decrease in energy from incident neutrinos. Interestingly, The decrease we see along the negative X axis in the experimental as well as full simulation histograms has a much sharper decrease along the same positional values when compared to all other plots.

We believe this severe loss along the negative X axis to be caused by the presence of a magnetic coil, positioned at X=0 in our coordinate system, running longitudinally down the length of the detector (Z axis), serving to attract decayed muons in order to track their trajectory through the detector. This coil has up until now been disregarded in our considerations, but we now notice an effect where the measured energy

spectrum of the beam as well as the model is affected by the presence of this coil. This is ascertained from contrasting the Mean v Position and Entry v Position plots in Figures 32 through 39 from the histograms created from both Experimental and Simulated histograms for the X axis and the corresponding ones for the Y axis.

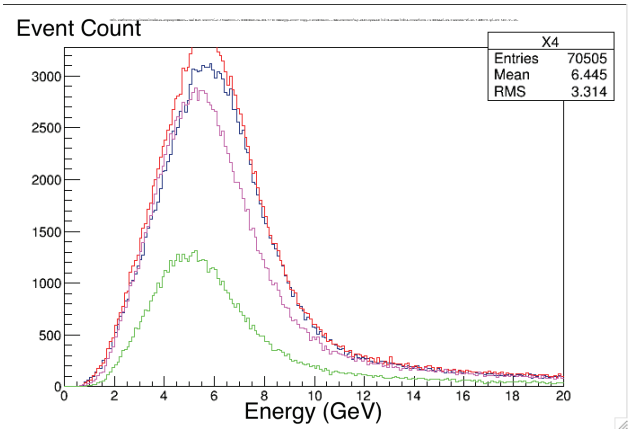

Figure 16: X Positive Experiment Unscaled

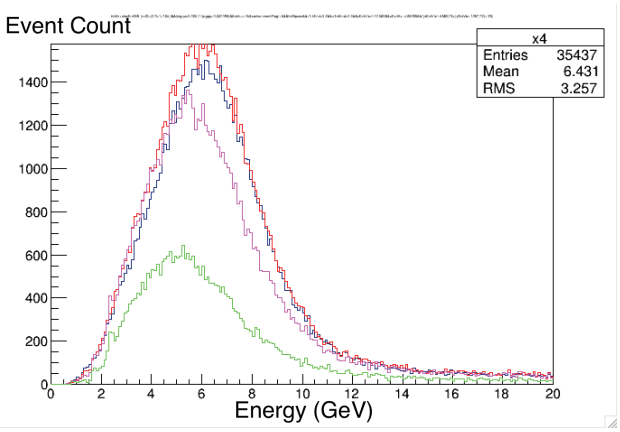

Figure 17: X Positive Simulation Unscaled

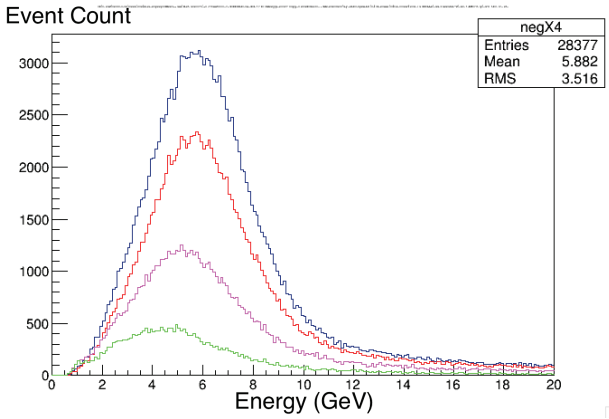

Figure 18: X Negative Experiment Unscaled

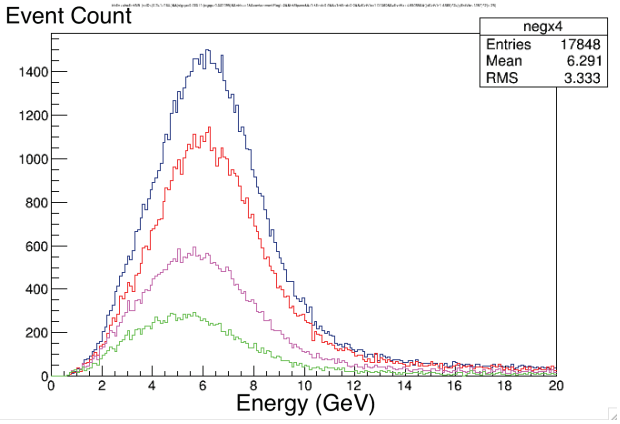

Figure 19: X Negative Simulation Unscaled

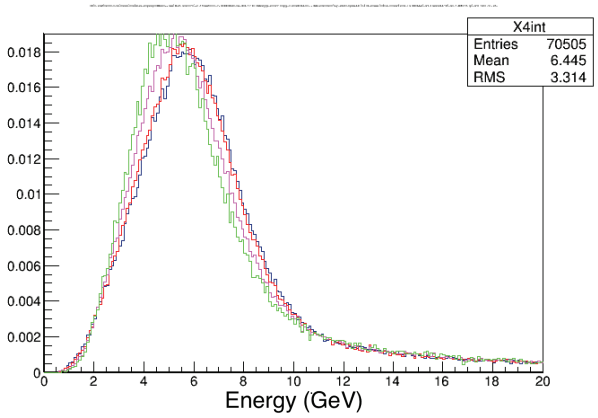

Figure 20: X Positive Experiment Scaled

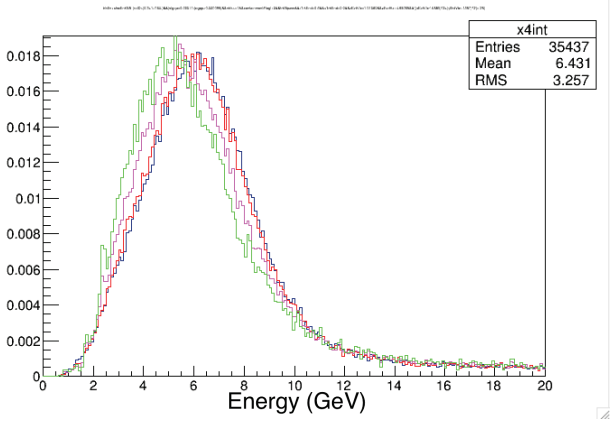

Figure 21: X Positive Simulation Scaled

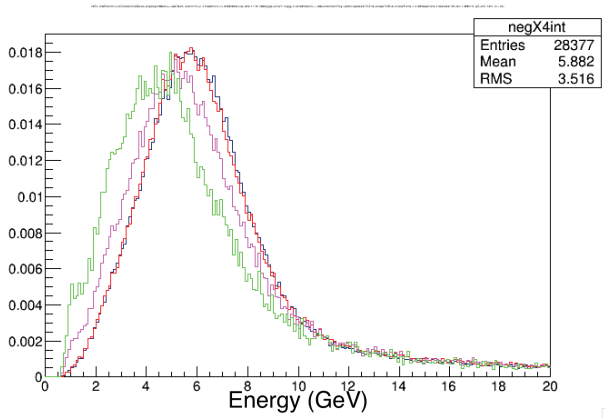

Figure 22: X Negative Experiment Scaled

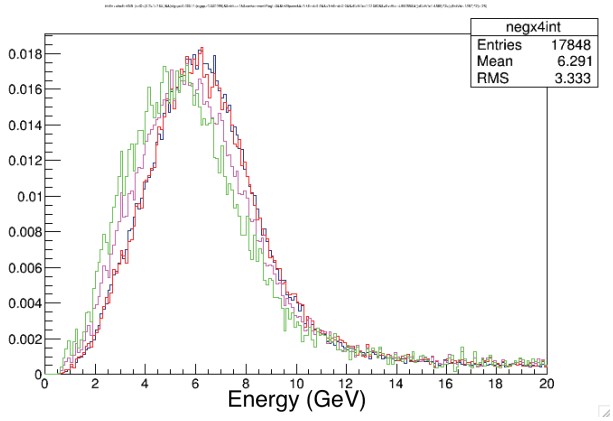

Figure 23: X Negative Simulation Scaled

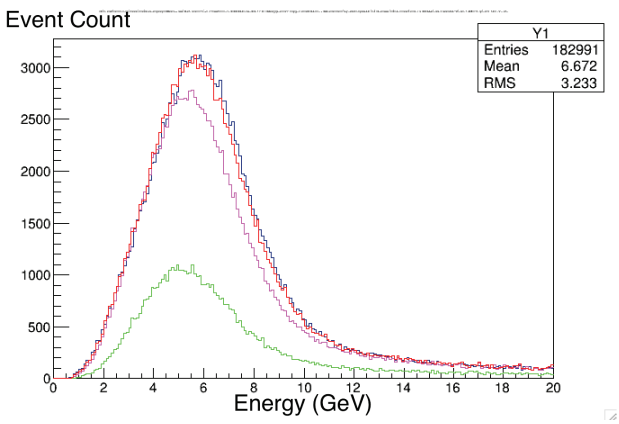

Figure 24: Y Positive Experiment Unscaled

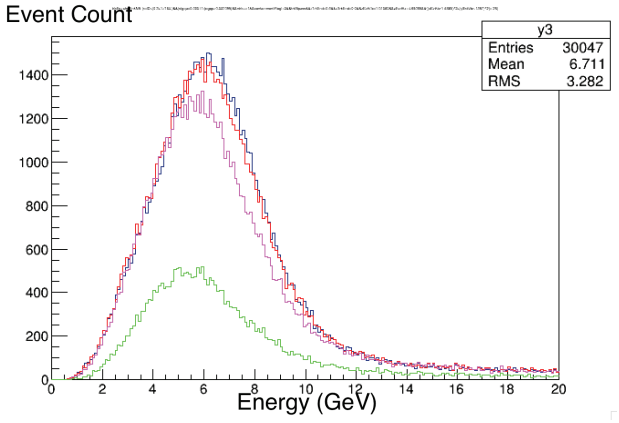

Figure 25: Y Positive Simulation Unscaled

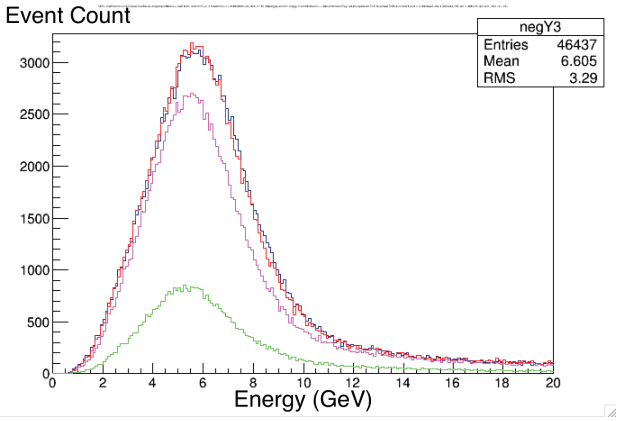

Figure 26: Y Negative Experiment Unscaled

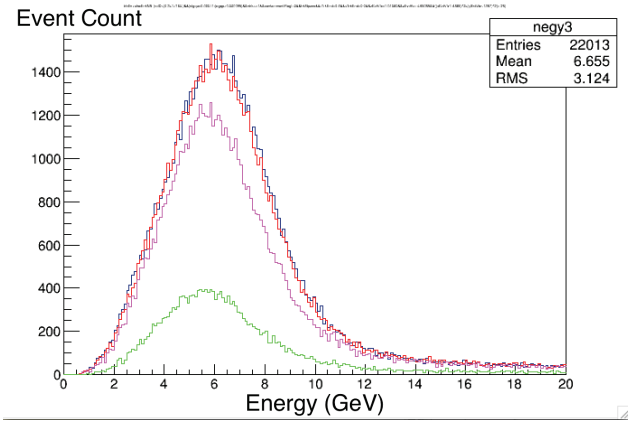

Figure 27: Y Negative Simulation Unscaled

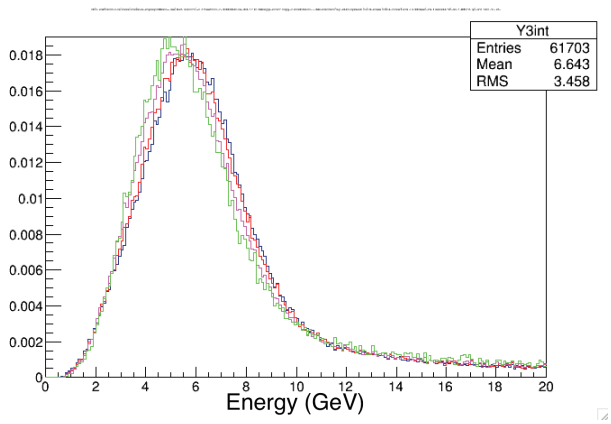

Figure 28: Y Positive Experiment Scaled

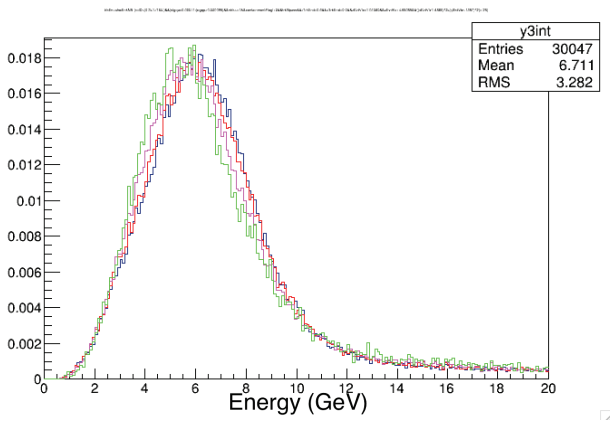

Figure 29: Y Positive Simulation Scaled

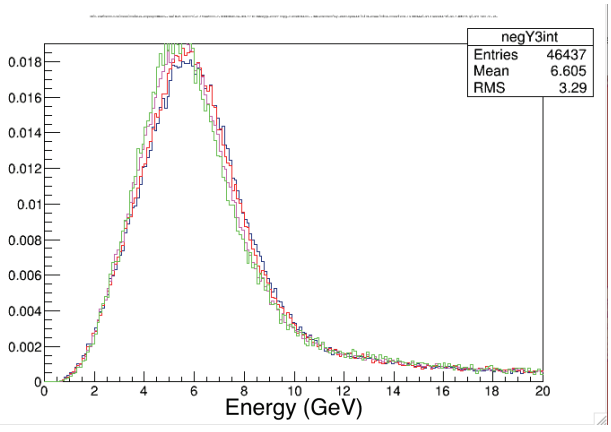

Figure 30: Y Negative Experiment scaled

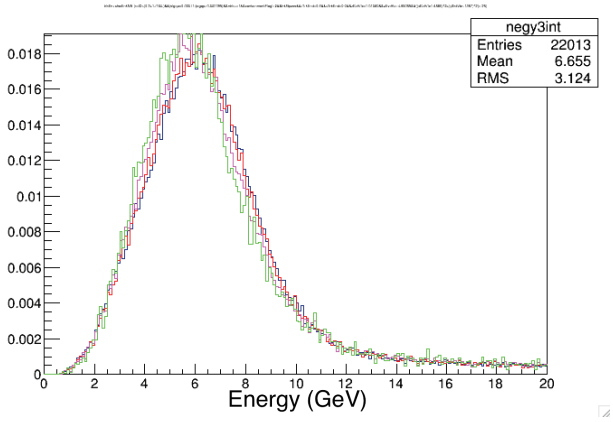

Figure 31: Y Negative Simulation scaled

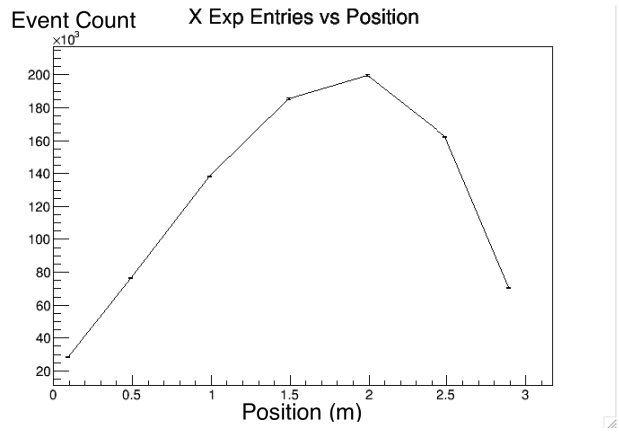

Figure 32: X Axis Entries vs Position for Experimental data.

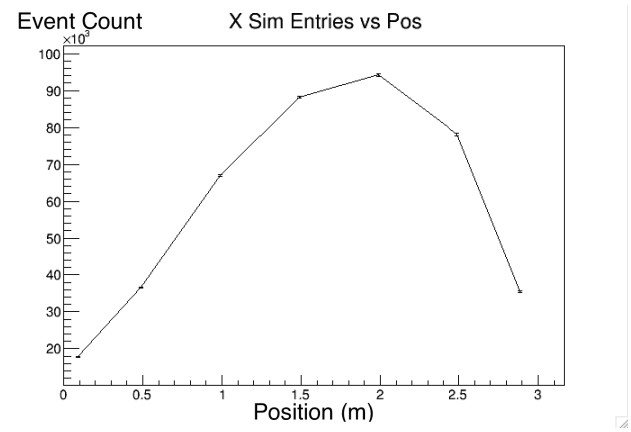

Figure 33: X Axis Entries vs Position for Simulated data.

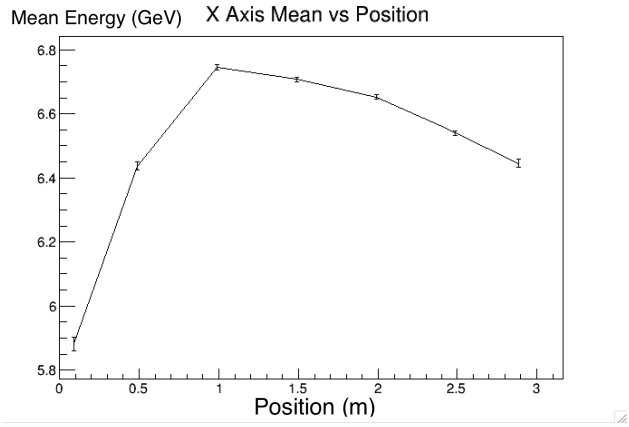

Figure 34: X Axis Means vs Position for Experimental data.

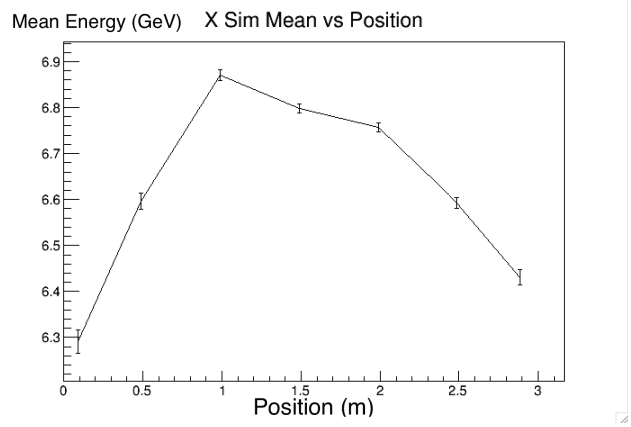

Figure 35: X Axis Means vs Position for Simulated data.

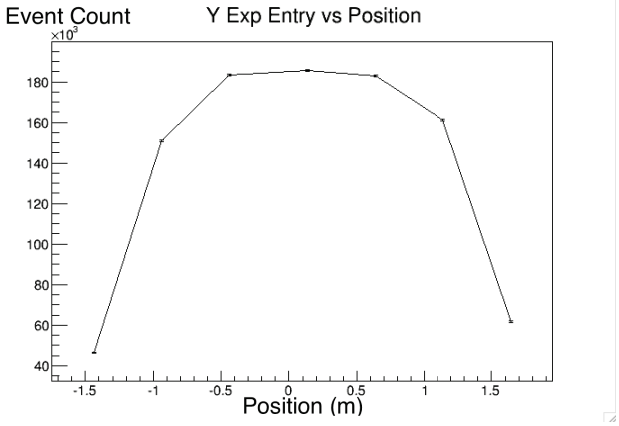

Figure 36: Y Axis Entries vs Position for Experimental data.

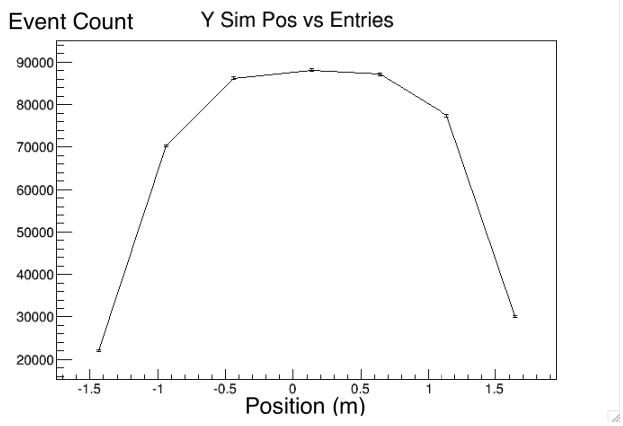

Figure 37: Y Axis Entries vs Position for Simulated data.

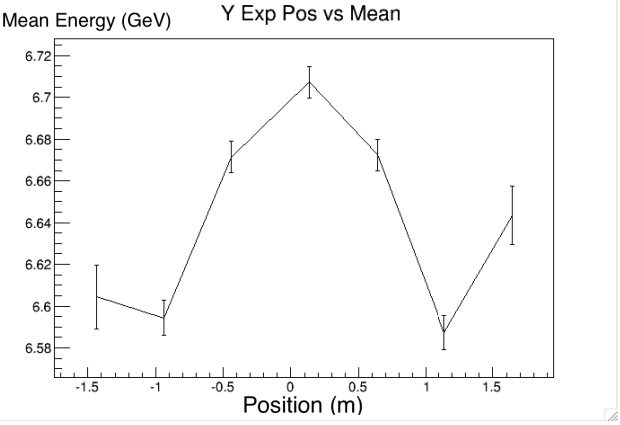

Figure 38: Y Axis Means vs Position for Experimental data.

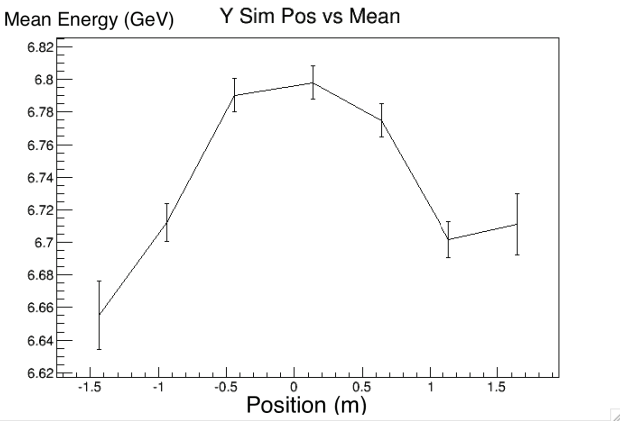

Figure 39: Y Axis Means vs Position for Simulated data.

Conclusion

We have successfully isolated the source of the initial error, understanding further and further which component of our model is deficient. Currently, we understand, based on the above information, that the inclusion of the magnetic coil inside the detector is responsible for a portion of the error. However, we also understand that modeling of the beam angle is producing a portion of error as it strays from the center axis of the beam, with deviation from experiment found exclusively in the longitudinal momentum component of the simulation. This presents us with a new challenge in discerning what part of the simulation is responsible for each of these two separate effects. We see in the data that both the mean Energy and number of events changes with position in the Near Detector, as expected from Equations 1 and 2. Some of this effect is likely due to the detector's magnetic field. Overall, these results are promising and with further analysis may point the way to improve the modeling of the NuMI beam.

References

[1] Kopp, Sacha E. *"Accelerator neutrino beams."* Physics reports 439.3: 101-159 (2007).

[2] G. Danby et al. *"Observation of High-Energy Neutrino Reactions and the Existence of Two Kinds of Neutrinos"*, Phys. Rev. Lett. 9, 36 (1962).

[3] P. Vahle. *"The MINOS Experiment"*, Presented at 13th International Conference on Topics in Astroparticle and Underground Physics (2013).

[4] MiNOS Collaboration *"The NuMI Neutrino Beamline"*, Paper to be published, courtesy of the MiNOS collaboration.